JACS
JOURNAL OF THE AMERICAN CHEMICAL SOCIETY
pubs.acs.org/JACS
Article

Dissecting the Essential Role of Anomeric β-Triflates in Glycosylation Reactions

Andrés G. Santana,[▽] Laura Montalvillo-Jiménez,[▽] Laura Díaz-Casado, Francisco Corzana, Pedro Merino, Francisco J. Cañada, Gonzalo Jiménez-Osés, Jesús Jiménez-Barbero, Ana M. Gómez, and Juan Luis Asensio*

Cite This: J. Am. Chem. Soc. 2020, 142, 12501−12514

Read Online

ACCESS | Metrics & More | Article Recommendations | Supporting Information

ABSTRACT: Glycosylations promoted by triflate-generating reagents are widespread synthetic methods for the construction of glycosidic scaffolds and glycoconjugates of biological and chemical interest. These processes are thought to proceed with the participation of a plethora of activated high energy intermediates such as the α- and β-glycosyl triflates, or even increasingly unstable glycosyl oxocarbenium-like species, among which only α-glycosyl triflates have been well characterized under representative reaction conditions. Interestingly, the remaining less accessible intermediates, yet to be experimentally described, seem to be particularly relevant in α-selective processes, involving weak acceptors. Herein, we report a detailed analysis of several paradigmatic and illustrative examples of such reactions, employing a combination of chemical, NMR, kinetic and theoretical approaches, culminating in the unprecedented detection and quantification of the true β-glycosyl triflate intermediates within activated donor mixtures. This achievement was further employed as a stepping-stone for the characterization of the triflate anomerization dynamics, which along with the acceptor substitutions, govern the stereochemical outcome of the reaction. The obtained data conclusively show that, even for highly dissociative reactions involving β-close ion pair (β-CIP) species, the formation of the α-glycoside is necessarily preceded by a bimolecular α → β triflate interconversion, which under certain circumstances becomes the rate-limiting step. Overall, our results rule out the prevalence of the Curtin−Hammett fast-exchange assumption for most glycosylations and highlight the distinct reactivity properties of α- and β-glycosyl triflates against neutral and anionic acceptors.

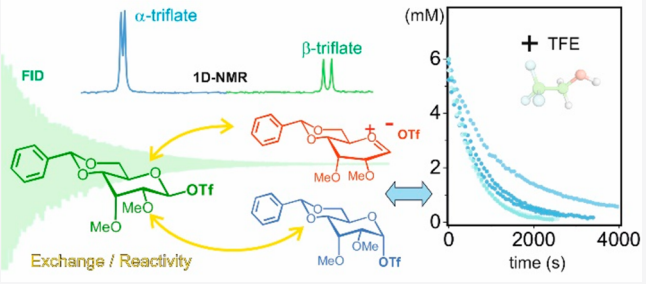

INTRODUCTION

The acknowledgment of the relevance of glycoconjugates in biological processes has run parallel to the development of new methods for glycosidic bond formation.[1−9] Thus, the last few decades have witnessed a burgeoning progress in the area of glycosyl donor engineering, with a more recent focus on the understanding of glycosylation mechanisms.[10−15] Central to many of these processes is the role played by glycosyl triflates. These highly reactive species are formed upon activation of common sugar donors, such as glycosyl sulfoxides or thioglycosides among others,[16] and are believed to exist as a mixture of α- and β- anomers in a fast exchange equilibrium. Both of them can, in turn, participate in nucleophilic substitutions with alcohol acceptors through a continuum of mechanisms spanning the gap between pure S_N2 and S_N1 processes, as shown by extensive studies performed by Crich and colleagues.[10] Owing to stereoelectronic and polar considerations, equatorially oriented anomeric triflates display a decreased stability with respect to their axial counterparts, as dictated by the anomeric effect.[17] However, while β-triflates are, at best, marginally populated, they can still play key roles in glycosylations due to their much enhanced reactivity. Indeed, a Curtin−Hammett scenario, implying a rapid α/β triflate interconversion on the reaction time-scale, has been traditionally invoked to describe glycosidic bond formation and to explain the stereoselectivity of the process (Figure 1a).[10] A paradigmatic example of this is provided by the diverging α- and β-selectivity observed in glycosylations with 4,6-*O*-benzylidene-protected D-glucopyranosyl and D-mannopyranosyl donors, respectively.

According to current knowledge, the decreased stability/population of the β-triflate intermediate for mannose derivatives, disfavored both by the anomeric effect and by repulsive dipolar interactions with the axial substituent at C2, would effectively thwart any Curtin−Hammett kinetic scheme, thus determining the preferential formation of the β-product via the

Received: May 20, 2020
Published: June 24, 2020

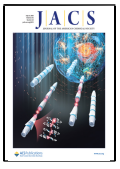

https://dx.doi.org/10.1021/jacs.0c05525
J. Am. Chem. Soc. 2020, 142, 12501−12514

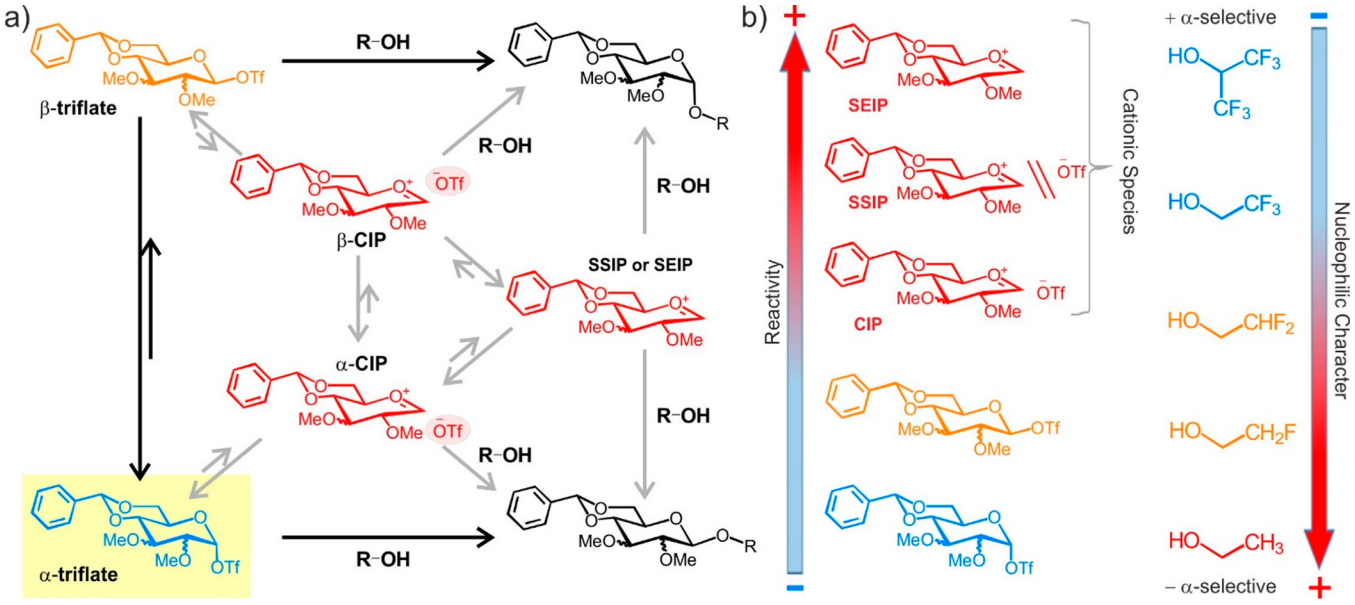

Figure 1. (a) Schematic representation of the multiple S_N2/S_N1 reaction pathways leading to the formation of α- and β-glycosides from glycosyl triflate intermediates. CIP, SSIP, and SEIP stand for contact ion pair, solvent separated ion pair, and solvent equilibrated ion pair, respectively. (b) Reactivity gradient for the potential donor intermediates and acceptor alcohols. Glycosylations with weakly nucleophilic alcohols proceed with increased α-stereoselectivity.

major α-triflate.[10] On the contrary, analogous glucose donors would evolve through a more accessible β-triflate to yield the corresponding inverted α-products. Interestingly, chemical glycosylations with poorly nucleophilic acceptors seem to proceed, in all cases, with an enhanced α-selectivity as shown by Codée and colleagues, which could reflect the dominant role played in these circumstances by the minor, yet more reactive intermediates, such as β-triflates or even glycosyl oxocarbenium-like species present in the reaction mixture (Figure 1b).[11a]

Notwithstanding the wide relevance of anomeric triflates in glycochemistry, very little is known about the anomerization process and its potential impact on the glycosylation outcome. More specifically, the NMR detection of the highly unstable equatorially oriented triflates has represented a significant challenge in itself, and just one example, involved in a conformational rather than an anomerization equilibrium, has been confidently reported so far.[18] However, key aspects of the mechanism, including triflate α/β exchange rates or their substitution kinetics by an alcohol, have proven inaccessible to the chemical community under direct experimental scrutiny, due to the marginal population and high reactivity of some of the species involved (Figure 1). In fact, it is important to emphasize that, in the absence of more detailed information, the general prevalence of Curtin–Hammett's conditions for these processes should be considered a mechanistic assumption. To address these issues, we have carried out a comprehensive analysis of anomeric substitutions involving α- and β-triflate species, focusing our attention on those reaction pathways that determine the formation of a major α-glycoside from a seemingly exclusive α-glycosyl triflate intermediate. With this objective in mind, we have employed a multidisciplinary approach comprising the extensive use of variable temperature NMR (vt-NMR) on both unlabeled and isotopically labeled samples, as well as competition and kinetics experiments, high-level computational chemistry calculations and preparative scale reactions.

RESULTS

Experimental Determination of Relative Glycosylation Rates. From a chemical perspective, the divergent stereoselectivities observed for the 4,6-*O*-benzylidene-protected epimeric donors **1a** and **2a** must reflect the distinct rates that characterize the alternative reaction pathways represented in Figure 1a. While a complete picture of the operating glycosylation mechanism is difficult to draw, relative formation rates for the α/β products can, in principle, be estimated by straightforward competition experiments. In order to gain insight into the differential reactivity and properties of the glucose/mannose dyad (**1a** vs **2a**, Figure 2a), two complementary assays (herein referred to as ***c-I*** and ***c-II***) were carried out, employing low temperature NMR (Figure 2b):

- In competitions type ***c-I***, glycosyl triflates derived from **1a** or **2a** (in separate assays), were treated with an equimolecular binary mixture of competing alcohols in significant excess, comprising a good nucleophile (ethanol) and a weakly nucleophilic acceptor (trifluoroethanol) (Figure 2b; green-shaded boxes). This kind of assay reveals the acceptor sensitivity displayed by each triflate. It is worth mentioning that analogous experiments were originally employed by Sinnott and colleagues for the study of glycoside solvolysis reactions and have since been used by other authors in different contexts.[19]
- On the contrary, in competitions type ***c-II***, an equimolecular mixture of competing triflates, derived from **1a** and **2a**, was treated with a substoichiometric amount of a given acceptor alcohol, either ethanol or trifluoroethanol (in separate experiments) (Figure 2b; yellow-shaded boxes). Under these experimental conditions, we should be able to determine the relative donor reactivity for each acceptor alcohol.

Each individual experiment (either ***c-I*** or ***c-II***) can yield a mixture of four glycosylation products whose population ratios, determined through 1D or 2D-HSQC spectra, indicate their

https://dx.doi.org/10.1021/jacs.0c05525
J. Am. Chem. Soc. 2020, 142, 12501–12514

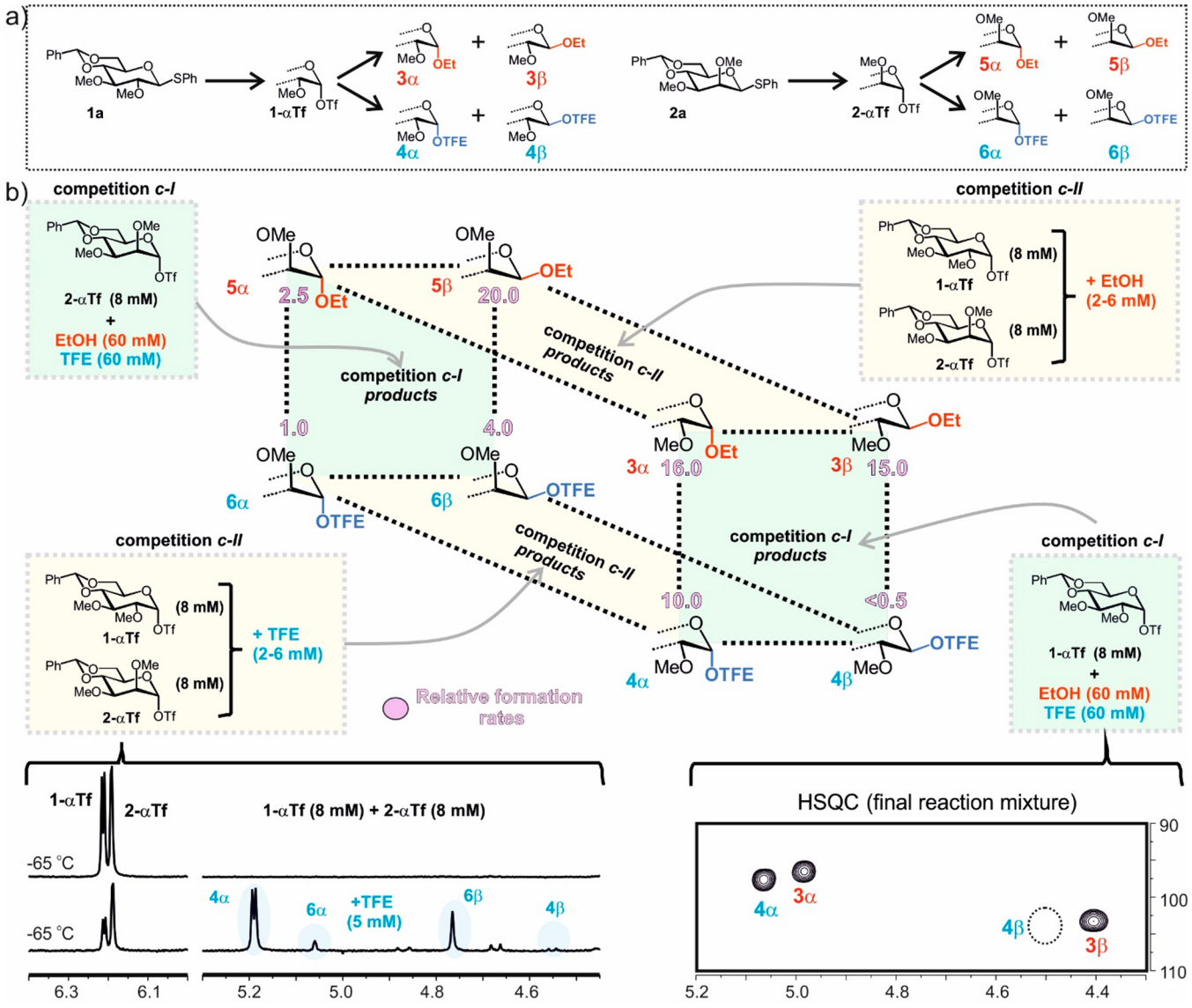

Figure 2. (a) Different chemical species involved in the competition experiments. (b) Competition experiments type *c-I* (green-shaded boxes) and *c-II* (yellow-shaded boxes) performed with donors **1-*α*Tf** and/or **2-*α*Tf** (initial concentrations shown in black), employing ethanol and/or trifluoroethanol (TFE) as acceptors (concentrations displayed in red and cyan, respectively). Relative populations for the products were determined by 1D and 2D-HSQC experiments (see the examples at the bottom) and allowed estimation of the relative formation rates for the eight possible glycosylation products. These values are represented in mauve.

relative formation rates. It should be noted that these values can reflect a mixture of processes and to some extent depend on the concentration of the reacting agents. However, they still provide valuable insights about the underlying reaction mechanism. Relative formation rates estimated for the eight possible glycosides generated, together with the experimental conditions employed for each assay, are represented in Figure 2 (see also Figure S1 of the Supporting Information, SI) and the main conclusions thereof are summarized in the following points:

- Regarding *β*-glycosylations, the replacement of ethanol by the weaker trifluoroethanol determines, in all cases, the expected reduction in the corresponding reaction rates (**3*β*** vs **4*β*** and **5*β*** vs **6*β***). Interestingly, this effect is much more pronounced for the glucose case (>20-fold), where the TFE-derived *β*-product was barely detectable in the reaction mixtures. On the contrary, both *α*-glycosylations seem fairly insensitive to the nucleophilic character of the acceptor alcohol, with relative rate decreases in the 1.6–2.5 range (**3*α*** vs **4*α*** and **5*α*** vs **6*α***). These latter results are fully consistent with experimental observations reported by Codée and colleagues according to which *α*-stereoselectivity increases for poor acceptors, and points to the involvement of more reactive species, either *β*-triflates or glycosyl oxocarbenium ions, in this particular reaction pathway.[11]
- With nucleophilic acceptors such as ethanol, both gluco- and manno- *β*-glycosides form with nearly identical rates (derivatives **3*β*** vs **5*β***). This is an unexpected conclusion, given the well-known *β*-selectivity of mannosyl triflates in contrast with the *α*-selectivity of its glucosyl counterpart. Therefore, the reason for the diverging stereochemical outcome of these two donors has to come from the *α*-glycosylation process, which indeed is significantly faster for the glucose derivative (ca. 6-fold, **3*α*** vs **5*α***), a trend

https://dx.doi.org/10.1021/jacs.0c05525
J. Am. Chem. Soc. 2020, 142, 12501−12514

that is further accentuated in the presence of weak alcohols (ca. 10-fold, ***4α*** vs ***6α***).

These initial studies confirm that the configuration of position 2 of the sugar donor is key in modulating the stereoselective outcome of the glycosylation process, probably by affecting the stability/population of the corresponding β-glycosyl triflates, and further support the participation of such intermediates in the process of α-glycosylation.

Comprehensive NMR Analysis of the Anomeric Substitution of Glucosyl Triflates by Poor Acceptors. With the results from the previous section in hand, we focused our attention on the intriguing behavior displayed by glucosyl donor **1a** with trifluoroethanol. As shown in Figure 2, this particular glycosylation proceeds with a total stereoselectivity to render an exclusive α-adduct from a predominant α-triflate intermediate, which would make the involvement of a highly reactive β-species even more relevant in this case. Importantly, while the existence of a β-glucosyl triflate has often been postulated, to the best of our knowledge, it has neither been detected, nor quantified before. Taking this into consideration, we first decided to have a closer inspection at the triflate mixtures generated from glucosyl donors under different glycosylation conditions.

NMR Detection of the β-Glucosyl Triflate Intermediate. In order to increase the chances to detect the key β-triflate intermediate, we resorted to ^{13}C-labeled samples. Thus, both the thio-phenyl derivative **1a** and the corresponding sulfoxide **1b** were synthesized from ^{13}C-glucose and preactivated at low temperature. The resulting solutions were analyzed by means of HSQC experiments (Figure 3a) and revealed the presence of an apparently exclusive α-triflate species (>99%), in agreement with previous reports.[10,16]

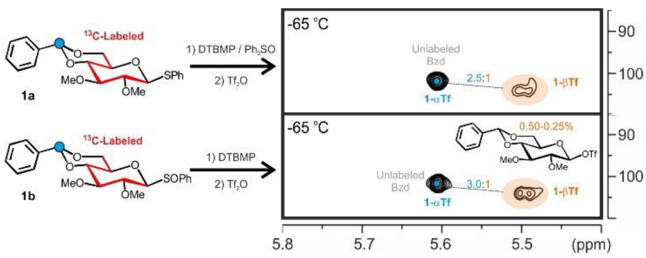

Figure 3. HSQC experiments acquired with triflate mixtures generated upon activation of ^{13}C-labeled donors **1a** and **1b**. Cross-peaks corresponding to the (unlabeled) benzylidene CH fragment in the major α-glucosyl triflate intermediate (in cyan), and the ^{13}C-labeled anomeric CH group in the corresponding β-glucosyl triflate (in orange) are shown. Peak relative ratios, together with the estimated population for the β-derivative are indicated.

In fact, despite the extra sensitivity provided by the isotopically labeled samples, significant accumulation times were required before an anomeric cross-peak could be confidently assigned to a β-triflate intermediate. This signal appears at δ_H = 5.48 ppm, around 0.6 ppm upfield shifted with respect to that of the major α derivative and presents a δ_C value of 104 ppm in chloroform (Table S1). In addition, both the homonuclear proton−proton ($^3J_{HH}$ = 7.2 Hz) and the heteronuclear proton-carbon ($^1J_{HC}$ = 177 Hz) coupling constants are in agreement with the equatorial orientation of the anomeric substituent. Satisfactorily, this result was successfully reproduced regardless of the activation protocol employed, inherent to each donor type (thiophenyl or sulfoxide donors, **1a** and **1b**). Finally, from the intensity of the detected cross-peaks, the β-triflate population was estimated between 0.25 and 0.50%, consistent with a $K_{\alpha\beta}$ equilibrium constant in the 2.5×10^{-3} to 5.0×10^{-3} range, which corresponds to a free energy difference of 2.3 ± 0.15 kcal/mol at −65 °C between the α- and β-triflates.

Kinetics of the α-Glucosylation Process with Poor Acceptors. The time evolution of the glucosyl triflate mixtures upon addition of trifluoroethanol was analyzed next. This represented a significant challenge from an experimental perspective, given the high reactivity and reduced stability of the triflate intermediates. However, a careful experimental design allowed us to handle these solutions with minimal temperature fluctuations during the whole process, particularly during the critical steps of adding the acceptor alcohol and mixing the resulting solution. Nevertheless, as an extra precaution to minimize the impact of any potential temperature changes on the reaction time courses, the first data point recorded in each experiment was discarded by default, and the initial concentrations reset accordingly.

Reactions were performed with increasing concentrations of trifluoroethanol (TFE), herein referred to as experiments ***A***−***E***, and monitored through sequential 1D-NMR spectra. Selected data sets, together with all reaction curves derived for this donor/acceptor pair, are shown in Figure 4a and b, respectively (see also, Figure S2). A visual inspection of curves ***A*** and ***B*** reveals that the process becomes faster with the acceptor concentration. Intriguingly though, this acceptor sensitivity diminishes in experiments ***B***−***C***, and totally vanishes for reactions ***D***−***E*** carried out with the highest trifluoroethanol/donor ratios (Figure 4b−d). Such observations seem inconsistent with the assumption of either a simple bimolecular or unimolecular mechanism, and points to a more complex scenario for the formation of the α-glycoside. Indeed, attempts to analyze the obtained curves assuming a first-order process yielded a poor fitting for data set ***A***, which progressively improved for curves ***B***−***E*** (Figures 4d and S3).

In view of these results, the experiments were re-examined in a more elaborate fashion, fully assuming the kinetic model represented in Figure 4c, which involves triflate anomerization prior to substitution of the resulting β-derivative with trifluoroethanol. Therefore, the system is defined by four rate constants, herein referred to as $k_{\alpha\beta}$ and $k_{\beta\alpha}$ for triflate anomerization, and $k_{G\alpha}$ and $k_{G\beta}$ for the alcohol substitution processes of each individual glucosyl-triflate. A least-squares fitting of the ten reaction curves was simultaneously performed with the program Dynafit[20] to determine the set of constant values which better agrees with all the experimental information available. Considering the significant nucleophilic character exhibited by triflate anions in organic solvents,[21] the anomerization step was assumed to be bimolecular, and the $k_{\beta\alpha}/k_{\alpha\beta}$ ratio was constrained to the experimentally determined value ($K_{\alpha\beta} = 3.3 \times 10^{-3}$). Regarding the second step, both zero and first-order kinetics in the alcohol were explicitly considered, but only the second mechanistic assumption produced satisfactory results (see Figures S4 and 4b, respectively). According to these data, the substitution of the α-glucosyl triflate with the acceptor alcohol is much slower than its conversion into the more reactive β-triflate ($k_{G\alpha} \ll k_{\alpha\beta}$), which is in agreement both with the negligible fraction of β-glycoside product generated in the process, and also with the higher nucleophilic character of the triflate anion with respect to trifluoroethanol.[21] On the contrary, the highly reactive β-triflate

https://dx.doi.org/10.1021/jacs.0c05525
J. Am. Chem. Soc. 2020, 142, 12501−12514

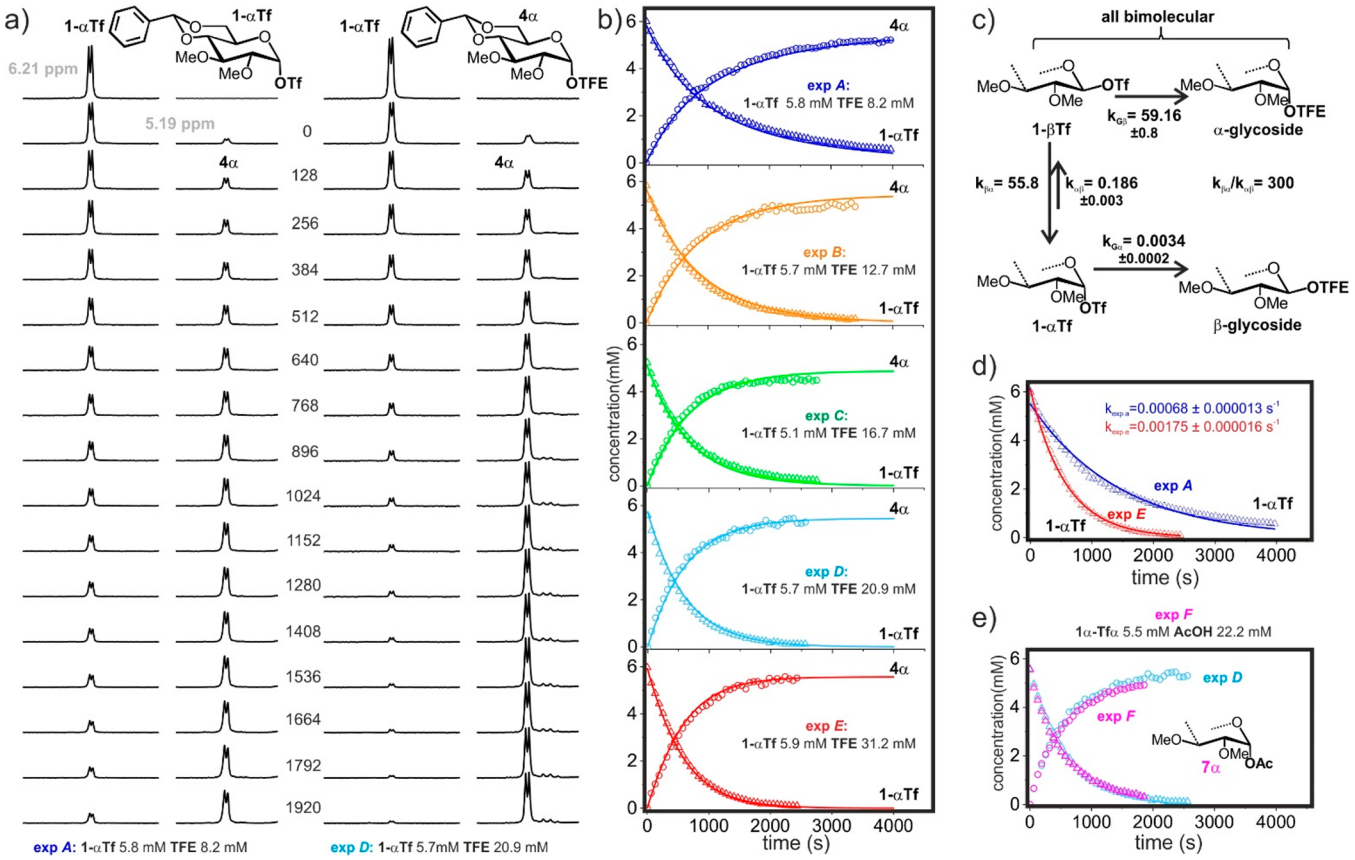

Figure 4. (a) Time evolution of **1-*α*Tf** in $CDCl_3$ at −65 °C upon addition of trifluoroethanol (experiments ***A*** and ***D***). (b) Experimental reaction curves (circles and triangles) derived from experiments ***A***−***E***. The solid lines represent the simultaneous least-squares fitting of the ten curves to the kinetic model shown on panel c. (c) Kinetic model employed for the analysis of the experimental reaction curves. The resulting kinetic constants are represented in black. During the fitting procedure the $k_{\beta\alpha}/k_{\alpha\beta}$ ratio was constrained to the experimentally determined range. (d) First-order fitting of reaction curves for the consumption of **1-*α*Tf** in experiments ***A*** and ***E***. (e) Experimental curves for experiment ***D*** superimposed on that derived from experiment ***F*** employing acetic acid as acceptor to yield derivative 7*α*.

intermediate shows no preference for any of these two species ($k_{G\beta}$~$k_{\beta\alpha}$), in line with the behavior observed in the ethanol/trifluoroethanol competitions ***c-I*** (vide supra). Strikingly, the resulting scenario, built on the obtained set of kinetic constants, does not satisfy Curtin−Hammett conditions, for which triflate exchange should be much faster than the acceptor substitutions ($k_{\alpha\beta} \gg k_{G\alpha}$ and $k_{\beta\alpha} \gg k_{G\beta}$). As a consequence, the α/β ratio for triflate intermediates cannot remain constant throughout the reaction, and so it must evolve during the process. More importantly, the global reaction rate can increase with the acceptor concentration up to a limit in which triflate anomerization becomes rate-limiting. In agreement with this view, glycosylations with TFE in the presence of additional triflate anion revealed a clear enhancement in the reaction rates which must partially reflect a faster anomerization process. Interestingly, these data sets also suggest additional activating effects of the triflate on the alcohol substitution step (Figure S5). Indeed, a catalytic influence of triflate anions on glycosylation processes has been recently reported.[14b]

This similar reactivity deduced for trifluoroethanol and anionic triflate against the *β*-glucosyl triflate is intriguing and made us wonder whether the same behavior stands for even weaker nucleophiles. With this idea in mind, we performed additional assays employing acetic acid as acceptor (Figure 4e, experiment ***F***; this assay did not include any base in the reaction mixture to ensure that no acetate form was present). Under these conditions, we observed that the reaction proceeds with total stereoselectivity to yield a sole *α*-*O*-acetyl-glycoside and that the obtained kinetic curves were almost identical to those previously recorded with a comparable concentration of trifluoroethanol (experiment ***D***), strongly suggesting a common reaction pathway (Figures S6).

While this model-based interpretation of the experimental data is plausible, the marginal *β*-triflate concentration present in the reaction mixtures renders key parameters of the kinetic scheme (such as the anomerization rate constants, $k_{\beta\alpha}$ and $k_{\alpha\beta}$) inaccessible by direct experimental measurements, thereby precluding further validation of our conclusions. At this point, we reasoned that an adequate redesign of the donor substrate, aimed at increasing the *β*-glycosyl triflate fraction in equilibrium, could provide definite support for the proposed kinetic regime.

Amplifying the *β*-Glycosyl Triflate Population through *α*-Selective Destabilizing Interactions: The Allose Case. In order to reduce the energy gap between both anomers, which ultimately determines the equilibrium populations, a simple strategy based on the destabilization of the *α*-glycosyl triflate by means of an unfavorable 1,3-diaxial interaction with a properly oriented substituent was employed. This approach was fully supported by quantum mechanics calculations carried out on the model structures (PCM(CHCl3)/M06-2*X*/6-31G(d,p)). Thus, according to theoretical data (Figure 5), the orientation of the C-2 substituent of the pyranose exerts a substantial influence on

https://dx.doi.org/10.1021/jacs.0c05525
J. Am. Chem. Soc. 2020, 142, 12501−12514

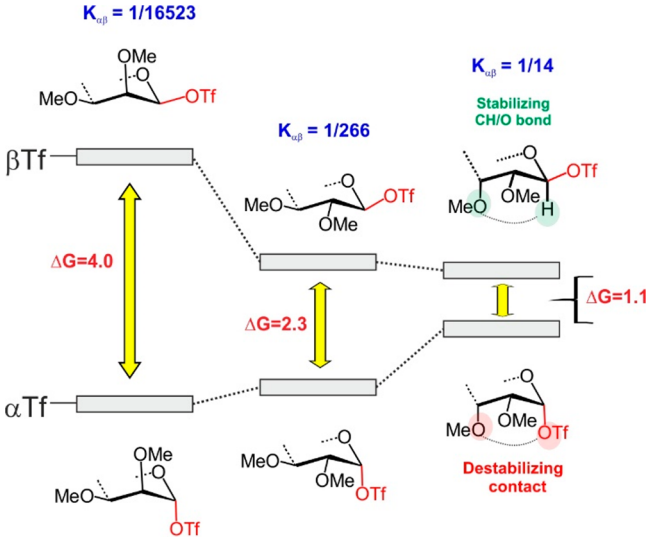

Figure 5. Free energy differences between α- and β-glycosyl triflates for D-manno-, D-gluco- and D-allo-derivatives (in the gas phase) computed by quantum mechanics calculations (PCM(CHCl3)/M06-2X/6-31G-(d,p)level). The predicted $K_{\alpha\beta}$ equilibrium constants are represented in blue.

the magnitude of the anomeric effect that decreases from manno- to gluco-configurations from 4.0 to 2.3 kcal/mol, in terms of free energy differences. It is worth mentioning that in the case of the glucose derivative, the calculated value shows a total agreement with the one experimentally estimated by us (2.3 kcal/mol; Figure 3).

As previously anticipated, the C-3 substituent offers the opportunity to further diminish the energy difference between anomers: an inversion of its orientation from equatorial to axial (such as in D-allose) leads to a severe polar/steric destabilization of the α-triflate, which in turn is accompanied by a slight stabilization of the β-anomer via a noncanonical CH−O hydrogen bond (a similar interaction has been previously proposed for α-equatorial triflates; Figure 5).[18] These combined effects would determine a sharp reduction of the α/β triflate energy gap, which becomes proximate to 1 kcal/mol and should therefore render the β-triflate amenable to experimental detection and characterization by NMR. Indeed, according to the obtained theoretical data, its population at −65 °C should be larger than 6%. The use of a larger basis set 6-311+G(2d,p) further increased the calculated stability of the β-triflate to yield a ΔG of 0.1 kcal/mol, and a β-triflate population around 45%.

Detection of the Allose β-Triflate Intermediate and NMR Characterization of the Exchange Dynamics. With this promising theoretical support in hand, we embarked in the preparation of D-allose donors **8a** and **8b**, which were preactivated employing regular conditions. To our satisfaction, low temperature NMR experiments confirmed, in both cases, the presence of an equilibrium mixture composed of α- and β-triflates in a 2.7:1 ratio, respectively, corresponding to a $\Delta\Delta G$ value of 0.4 kcal/mol at −65 °C (Figures 6a and S7).

The signal of the anomeric proton of the β-allosyl triflate appears at δ_H = 5.74 ppm, ca. 0.3 ppm downfield shifted with

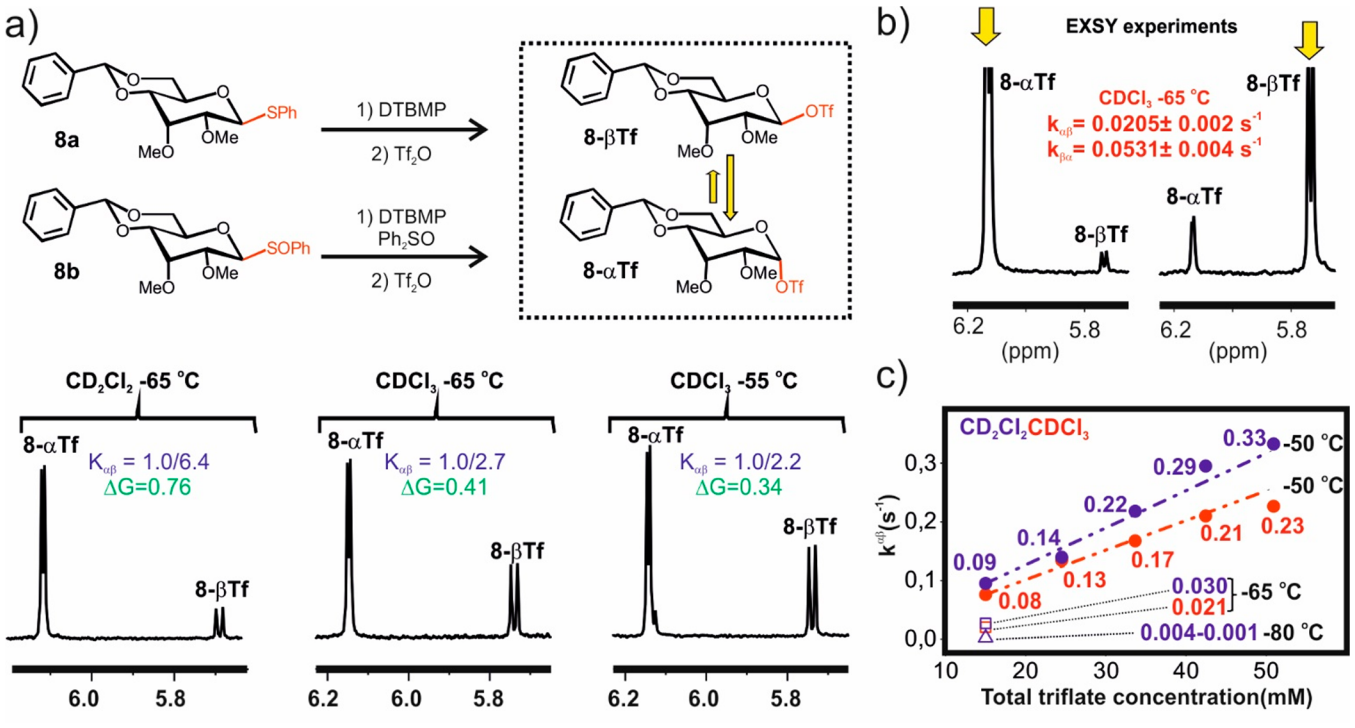

Figure 6. (a) Relative equilibrium concentrations for the α- and β-allosyl triflates (**8-αTf** and **8-βTf**) generated from donors **8a** or **8b**, in CD_2Cl_2 and $CDCl_3$, as revealed by 1D-NMR (for additional solvent or temperature conditions see Figure S8). The resulting $K_{\alpha\beta}$ and ΔG (kcal/mol) values are indicated. (b) Example of selective NOESY-1D experiments acquired with excitation of either the α or β anomeric signals (left and right, respectively). EXSY plots provided the rate constants, which were independently determined for the $\alpha \rightarrow \beta$ and $\beta \rightarrow \alpha$ processes and are represented in red. (c) Anomerization rate constants determined under different experimental conditions (solvent, temperature and triflate anion concentration). The horizontal axis represents the absolute concentration of the triflate anion in the reaction media, including contributions from the activating triflic anhydride and the added TBAOTf.

https://dx.doi.org/10.1021/jacs.0c05525
J. Am. Chem. Soc. 2020, 142, 12501−12514

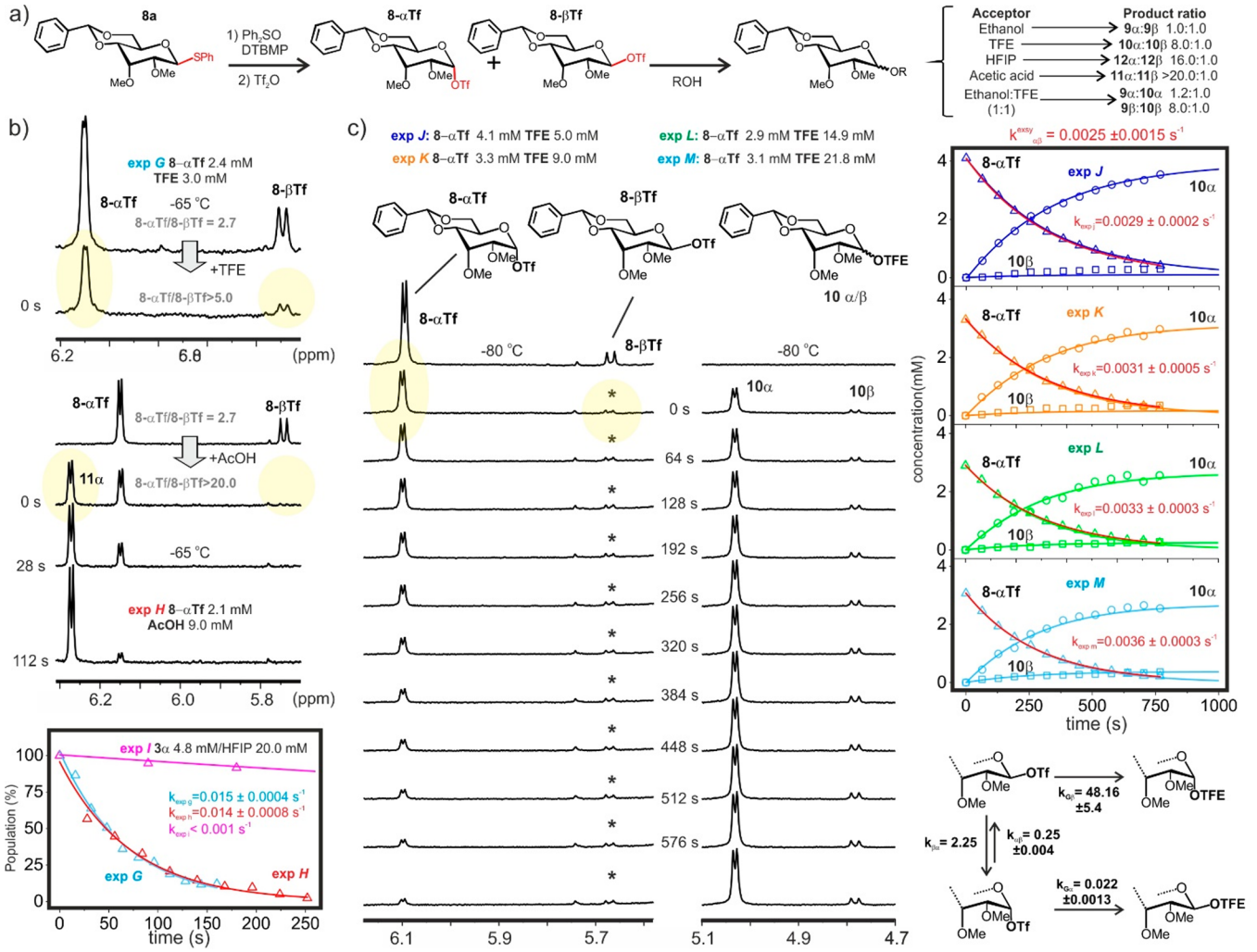

Figure 7. (a) Product ratios obtained upon treatment of triflates **8-*α*Tf** + **8-*β*Tf** with different acceptors or acceptor mixtures (competition type ***c*-*I***, last entry). (b) Kinetics experiments ***G*-*I*** (initial **8-*α*Tf** and acceptor concentrations indicated) performed in $CDCl_3$ at −65 °C. Selected 1D data sets, before and after addition of the acceptor (TFE or acetic acid), are shown. The anomeric triflate ratios (represented in gray) reveal the preferential consumption of the *β*-stereomer by the acceptor. Reaction curves for the consumption of the major *α*-allosyl triflate **8-*α*Tf**, together with the corresponding first-order fittings and rate constants derived thereof are shown at the bottom. (c) Kinetics experiments ***J*−*M*** performed in CD_2Cl_2 at −80 °C (initial **8-*α*Tf** and acceptor concentrations indicated). The time evolution of the allosyl triflate mixture in experiment ***J*** as monitored by 1D NMR is displayed on the left. Reaction curves derived from experiments ***J*−*M*** are represented on the right. First-order fittings and rate constants are shown in red. The solid colored lines represent the simultaneous least-squares fitting of the 12 curves to the kinetic model shown at the bottom-right corner. The resulting kinetic constants are represented in black.

respect to that previously detected for its glucose analog (Figure 3), probably reflecting its polar interaction with the axial methoxy group. However, both $^3J_{HH}$ and $^1J_{HC}$ constants for the anomeric position were fully consistent with those measured for the analogous *β*-gluco- intermediate (8 and 178 Hz, respectively). Interestingly, all measurable $^3J_{HH}$ values are in agreement with a $^4C_1$ conformation for both anomers, evidencing no significant distortions even for the *α*-derivative, where a steric conflict seems clearer (Figure S7 and Table S2). Additionally, to further interrogate this previously undetected anomerization equilibrium, both its temperature and solvent dependence were also studied. As expected, considering the reduced dipole moment exhibited by the *β*-anomer, its molar fraction increases in low dielectric environments (from *α*/*β* 6:1 in CD_2Cl_2 to 2.3:1 in toluene-*d*8). Similarly, the *α*/*β* ratio at equilibrium is tilted in favor of the less stable *β*-anomer at higher temperatures (Figures 6a and S8). In summary, according to our data, the fraction of *β*-triflate available for glycosylation shows a significant sensitivity to the experimental conditions employed, being the solvent polarity and the temperature two key parameters to consider.

The unusually large *β*-triflate population exhibited by the allose system offered the possibility of characterizing, also for the first time, the glycosyl triflate exchange dynamics. This anomerization process is central to the Curtin−Hammett schemes typically invoked to explain glycosylations. Fittingly, both 1D and 2D-EXSY experiments confirmed the presence of exchange peaks between *α*- and *β*-triflate intermediates, which allowed the determination of the corresponding rate constants under a variety of experimental conditions (Figures 6b and S8−S12).[22] Both $k_{\alpha\beta}$ and $k_{\beta\alpha}$ were independently measured following a protocol analogous to that described by Gschwind[22a] and Taylor,[22b] and the rate constant ratios ($k_{\beta\alpha}/k_{\alpha\beta}$) were found to be consistent with the corresponding experimental equilibrium constants (K_{eq}).

https://dx.doi.org/10.1021/jacs.0c05525
J. Am. Chem. Soc. 2020, 142, 12501−12514

Several conclusions can be obtained from these data. First, the exchange rates determined for D-allopyranosyl triflates in chloroform at −65 °C are 1 order of magnitude higher than those described for unconstrained glycopyranosyl mesylates at 25 °C, which shows the extreme lability of the former reactive species (see Figure 6b and Table S3).[22b] Second, resulting from the increased polarity of dichloromethane, whose influence on triflate equilibrium is already clear (Figure 6a), the experimental exchange rate values derived in this media are slightly larger than those measured in chloroform. Further, this process shows a great sensitivity to temperature, becoming 5-fold faster by simply raising the temperature to −50 °C. Conversely, the obtained experimental data is consistent with an almost 10-fold reduction in the exchange rate constant at −80 °C in dichloromethane (Figures S8−S12 and Table S3).

Most importantly, experiments carried out in the presence of increasing concentrations of tetrabutylammonium triflate (TBAOTf) at −50 °C and at −65 °C demonstrated that the exchange kinetics depend linearly on the triflate anion concentration in both solvents, with a slope that fully supports a bimolecular S_N2-like anomerization mechanism (Figures 6c and S8−S12 and Table S3). This observation agrees with the significant nucleophilic character of triflate anions in apolar environments[21] and implies that the apparent exchange rates derived from EXSY NMR data using the initial rate approximation[22a] correspond, in fact, to the product between the actual bimolecular constants and the concentration of triflate anion available for each assay (see the Experimental Methods). Therefore, true S_N2 rate constants (now expressed in M^{-1} s^{-1}) could be inferred, and the resulting values are also included in Table S3.

As a final point, the relevance of the obtained values under actual glycosylation conditions was tested, for which hexafluoroisopropanol (HFIP) was employed as the acceptor counterpart. By virtue of the slow progression of this reaction (vide infra), we were able to acquire quick EXSY NMR experiments during the process (Figure S13), showing that the triflate exchange dynamics previously described remain basically unaltered in the presence of the acceptor alcohol.

Chemical Characterization of the Allosyl Donor: Selectivity and Reaction Kinetics. The unusually large β-triflate population exhibited by the activated **8a** donor mixtures would be expected to have a significant impact on its reactivity in glycosylations. Thus, we carried out assays with a selection of representative weakly nucleophilic acceptors and the obtained results are compiled in Figure 7a. As it can be observed, the marked α-preference exhibited by the analogous glucose derivative with trifluoroethanol is slightly reduced in this case by the inversion of the pyranose position 3. This can be rationalized by an enhanced reactivity of the corresponding α-allosyl triflate, now capable of reacting sluggishly with this alcohol (**10α**:**10β** 8:1 compared with **4α**:**4β** > 20:1). Nevertheless, as previously shown for the glucose/mannose case,[11a] further attenuation of the acceptor nucleophilic character (from trifluoroethanol to hexafluoroisopropanol or acetic acid) should favor α-glycosidation, and indeed, in these two additional cases, the reaction proceeds with a total α-stereoselectivity (Figure 7a).

Type ***c-I*** competitions with ethanol/trifluoroethanol mixtures also revealed a similar behavior to that observed for glucose and mannose derivatives: the α-allosylation displays an almost null sensitivity to the acceptor, while the β-glycosylation remains significantly sensitive (Figure S14). Alternatively, competitions type ***c-II***, carried out with **1-Tf**/**8-Tf** triflate mixtures, showed that the formation rates of the allose products are at least 10-fold faster in comparison to those derived from glucose, regardless of the anomeric configuration of the product or the nature of the accepting alcohol. Overall, this reactivity enhancement must be reflecting both the destabilizing influence exerted by allose axial substituent on the α-triflate, and the concomitant growth in the β-triflate population.

Next, we analyzed the time evolution of the allose triflate mixtures upon addition of poor acceptors, such as trifluoroethanol or acetic acid at −65 °C in chloroform. The obtained results are represented in Figures 7b, S15, and S16 (experiments ***G*−*H***) and highlight several key features of the glycosylation process. Thus, the ratio between α- and β-triflate populations is not maintained throughout the experiment, owing to the fact that the minor β-triflate is preferentially consumed, at a rate too large to permit its monitorization by NMR. This observation shows that the reactivity difference between both anomers is significant despite the relatively small energy gap between them. Most importantly, the substitution of the β-triflate by the acceptor must be faster than the triflate anomerization, thus confirming that the glycosylation process cannot be described in terms of the Curtin−Hammett principle, as previously deduced for glucose donors.

The integration of anomeric signals for both the α-triflate intermediate and the products allowed us to build the corresponding reaction curves (Figure 7b). Interestingly, first-order analysis of these data sets yielded good fittings with rate constants highly similar to those previously derived for the α → β anomerization process (0.014−0.015 vs 0.013−0.024 s^{-1} (see Table S3). This experimental evidence establishes a mechanistic connection between the formation of the α-glycoside and the triflate exchange process and supports the notion that this latter step must be both essential and rate-limiting.

Conversely, glycosylation assays with the extremely deactivated HFIP (experiment **I**) evolve at a much-reduced rate, although with an exquisite α-stereoselectivity. Meaningfully, the relative populations of the α- and β-allosyl triflates remain unaltered throughout the reaction. These combined observations have two key mechanistic implications: on the one hand, the substitution of the β-triflate intermediate with this alcohol is slower than the exchange between allosyl triflates, in a way that the whole process now satisfies Curtin−Hammett requirements (see Figure S17). It should be noted though that this behavior is anecdotal and will certainly not hold for most of the alcohols commonly employed in glycosylation reactions. On the other hand, the conversion of the β-triflate into the major α-product is shown to respond to the substantial attenuation of the nucleophile (TFE vs HFIP), a plausible argument in favor of a bimolecular-like behavior for the substitution mechanism during this step.

Given the high reactivity exhibited by the allose donor with trifluoroethanol, we decided to carry out additional assays at even lower temperatures (−80 °C in CD_2Cl_2). These experimental conditions determined a slower progression of the reactions, allowing a more adequate monitorization of the experimental time courses. Analogously to the glucose case, reaction curves were derived at increasing concentrations of the acceptor alcohol (herein referred to as experiments ***J*−*M***). The obtained results represented in Figures 7c, S18, and S19 were consistent with the qualitative description of the glycosylation reaction previously outlined. Consequently, the β-triflate intermediate is preferentially consumed in all cases. Moreover, individual first-order analysis of the reaction curves (either for

https://dx.doi.org/10.1021/jacs.0c05525
J. Am. Chem. Soc. 2020, 142, 12501−12514

the consumption of the α-allosyl triflate or the formation of the α-product) renders rate constants in the range of those previously measured for the triflate exchange under similar experimental conditions (Table S3). Furthermore, the reaction rate shows only a slight sensitivity to the acceptor concentration, which for the dominant α-anomer could be attributed to the rate-limiting character of the preceding anomerization step, although a more S_N1-like alcohol association cannot be ruled out either.

In order to derive the set of kinetic constants that better reproduces all the experimental data, the obtained reaction curves were simultaneously fitted to the more elaborate kinetic scheme shown in Figure 7c. According to previous experimental evidence, we decided to consider both S_N2 and S_N1 scenarios for the alcohol substitution reactions. Contrarily, the exchange between α and β allosyl-triflates was taken as a pure S_N2 process, in accordance with the linear dependence on the triflate concentration revealed by NMR data previously shown (Figure 6c and Table S3). Therefore, the corresponding kinetic constants for this latter step ($k_{\alpha\beta}$ and $k_{\beta\alpha}$) were constrained to the experimentally derived values during the fitting procedure. Slightly better fitting results were attained by considering acceptor reactions with the β- and α-triflate intermediates as bimolecular processes. However, kinetic constants derived with the alternative mechanistic assumption, that is unimolecular, would still be consistent with the conclusion previously outlined (Figures S20 and S21): the formation of the major α-glycosylation product is rate-limited by the interconversion between α- and β-glycosyl triflates, in this case, even at roughly stoichiometric trifluoroethanol concentrations. This behavior results from the peculiar reactivity of the β-allosyl triflate intermediate whose substitution with the acceptor alcohol seems clearly favored over the one involving anionic triflate.

Primary ^{13}C-Kinetic Isotope Effect (KIE) Analyses for the Glucose and Allose Cases. As a next step, to get further insights into the reaction mechanisms, the primary ^{13}C-KIEs for both dominant products, the α-glucoside (**4α**) and the α-alloside (**10α**) formed with trifluoroethanol, were determined employing the NMR method originally proposed by Singleton[23] and later adapted by Crich[10d] for low temperature chemical glycosylations. Individual values measured at three different reaction conversions, together with the corresponding average are represented in Table 1 (see also Tables S4 and S5). It should be noted that according to the kinetic model considered in Figures 4c and 7c, both ^{13}C-KIE values could, to some extent, have contributions arising from both the triflate anomerization and the subsequent alcohol trapping, thus making an in-depth analysis of these single values not straightforward. Notwithstanding, they can still be employed for comparative purposes as similar reactions have been already analyzed by this method. Thus, for the glucose case the ^{13}C-KIE value determined (1.012) lies significantly closer to the range expected for S_N1-like substitutions (1.00−1.01), rather than to concerted S_N2 reactions (1.03−1.08). Comparatively, a ^{13}C-KIE of 1.023 has been reported for the α-glycosylation of the same triflate intermediate with isopropanol.[10d] According to these data, the replacement of isopropanol by a poorer nucleophile determines a shift in the reaction mechanism toward a more dissociative process, as proposed by Codée and Crich.[10,11a,b]

Table 1. Experimentally Determined Primary ^{13}C-KIEs[a]

conversion (%)	**4α**
11%	1.013
15%	1.012
21%	1.010
average	1.012 ± 0.002
conversion (%)	**10α**
6%	1.004
15%	1.005
20%	0.998
average	1.002 ± 0.004

[a]Obtained values for the α-glucopyranoside **4α** and the α-allopyranoside **10α** were measured at −65 °C ($CHCl_3$) and −80 °C (CH_2Cl_2), respectively, with three different reaction conversions. From them, the corresponding values at 25 °C were calculated.

Regarding the allose model, the obtained value (1.002) points to an even more dissociative process involving, most likely, the participation of a contact ion pair (β-CIP), which could be explained by a combination of factors. First, the axially oriented methoxy group at position 3 could favor contact ion pair formation by stabilizing the positive charge located at the anomeric position via through-space polar interactions.[24] Second, the large fraction of the β-allosyl triflate in equilibrium must also determine a higher population of the corresponding β-CIP, the species presumably involved in the substitution process.

Overall, the obtained results for both glycosylation processes suggest the participation of discrete short-lived oxocarbenium-like intermediates, structurally related with the corresponding parent β-glycosyl triflates. However, despite the dissociative character attributed to the reactions involving such intermediates, our results seem to imply that the alcohol is still involved in a kinetically significant way, on the basis of the sensitivity exhibited by the reaction rates to both the nucleophilicity and the concentration of the acceptor.

Quantum Mechanical Calculations. With the aim of further dissecting the interplay between triflate anomerization and the alcohol substitution processes we analyzed the ground/transition states involved by quantum mechanical calculations (see Computational Details), considering both ethanol and trifluoroethanol as acceptor alcohols. Computed energies and geometries are represented in Figure 8. Some clear trends are apparent from these data: first, the formation of the β-glycosides from the corresponding α-triflates via a direct inversion mechanism proceeds, in all cases, through high energy TSs (herein referred to as $TS_{G\beta}$; Figure 8), which are significantly more unfavored for the trifluoroethanol-involving reactions. Conversely, α-glycosylation processes show lower activation barriers and much reduced sensitivities to the nucleophilic character of the alcohol, in agreement with the competition experiments reported above. Additionally, TSs involved in triflate anomerization and α-glycosylations (named TS_{Exch} and $TS_{G\alpha}$, respectively) display comparable stabilities. Indeed, for the allose case, a considerable deviation from the Curtin−Hammett scenario is correctly anticipated, reflecting the balance between assisting and opposing influences of the pyranose axial substituent on both processes. Certainly, while this methoxy group stabilizes $TS_{G\alpha}$ by means of a hydrogen bonding interaction with the incoming alcohol, it destabilizes TS_{Exch} through repulsive interactions with the anionic triflate nucleophile. This is in good agreement with the experiments herein reported, which show that the relative stability between $TS_{G\alpha}$ and TS_{Exch} is, in fact, even more tilted in favor of the former, with $\Delta G^{\ddagger}_{G\alpha} \approx \Delta G^{\ddagger}_{Exch}$ for glucose (Figure 4) and $\Delta G^{\ddagger}_{G\alpha}$

https://dx.doi.org/10.1021/jacs.0c05525
J. Am. Chem. Soc. 2020, 142, 12501−12514

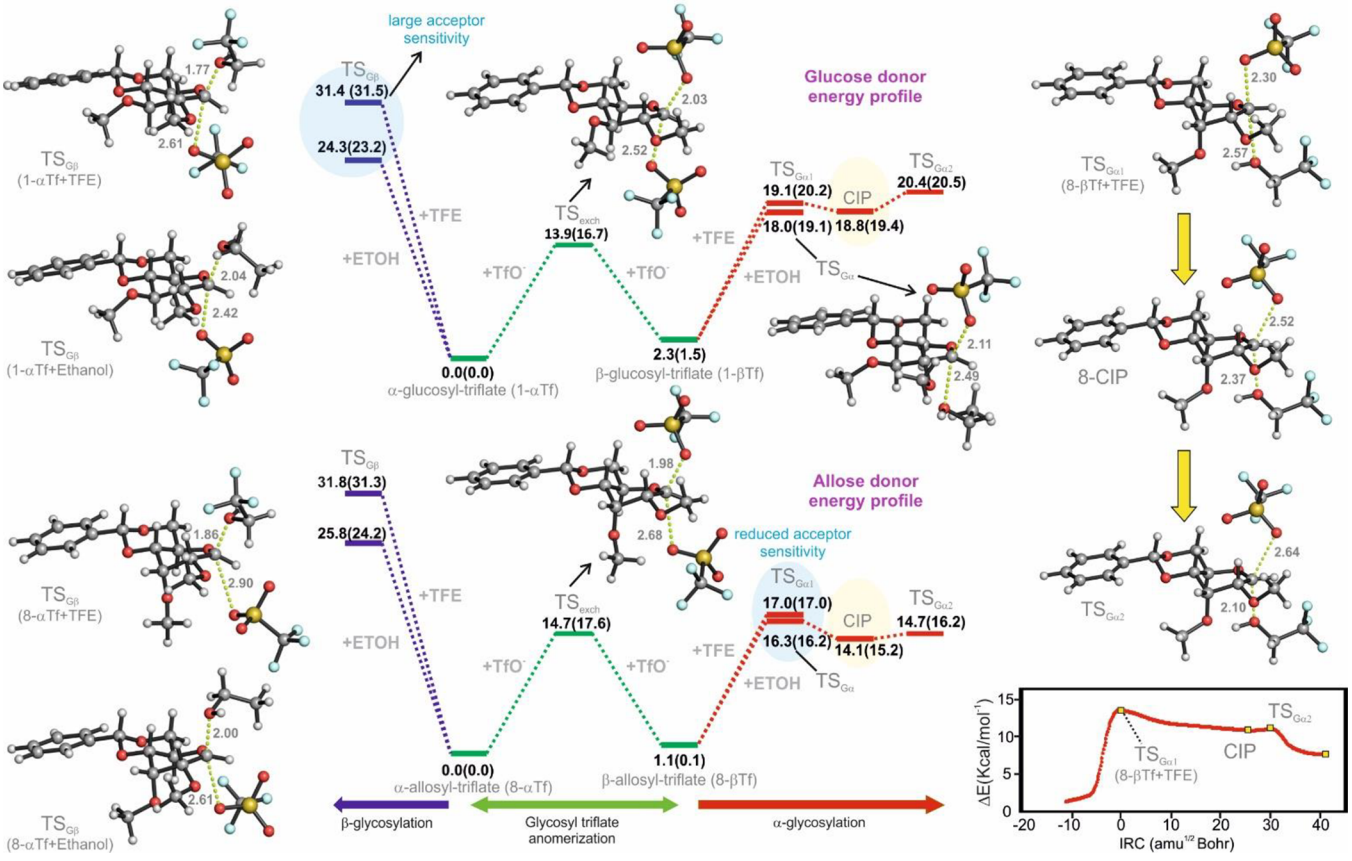

Figure 8. Relative stabilities for the transition states and intermediates involved in the anomeric substitution of glucosyl (up) and allosyl (down) triflates with ethanol and trifluoroethanol (employed notation is shown below), evaluated by quantum mechanics. Computed geometries for selected transition states and intermediates are also represented. The reaction coordinate calculated for the anomeric substitution of the β-allosyl triflate with trifluoroethanol is shown at the bottom-right corner, together with the geometry of the pertaining TSs/intermediates along this path (above). Geometries and intrinsic reaction coordinates (IRC) were calculated with PCM($CHCl_3$)/M06-2X/6-31G(d,p). Relative free energies (ΔG and $\Delta G^{\ddagger}$) are given in kcal/mol and interatomic distances in angstroms. Relative stabilities derived through single-point energy calculations at the SMD($CHCl_3$)/M06-2X/6-311++G(2d,p)//PCM($CHCl_3$)/M06-2X/6-31G(d,p) level are shown in parentheses.

$<\Delta G^{\ddagger}_{Exch}$ for allose (Figure 7). Of note, single-point energy calculations with SMD($CHCl_3$)/M06-2X/6-311++G(2d,p) improved the results observed at the PCM($CHCl_3$)/M06-2X/6-31G(d,p) level used for geometry optimizations and correctly reproduced the trend observed experimentally: triflate exchange is the rate-limiting step for allose, thus making the α-glycosylation rate almost independent of the nature of the accepting alcohol within this range. It is important to mention that the inversion of pyranose configuration at position 3, from D-gluco- to D-allo-, effectively diminishes the energy gap between α- and β-glycosyl triflates, as shown experimentally. However, a slower triflate anomerization is predicted for the allose case in both the $\alpha \rightarrow \beta$ and $\beta \rightarrow \alpha$ directions. This is only in partial accordance with our experimental data, which revealed a faster $\alpha \rightarrow \beta$ inversion for the α-allosyl triflate.

Regarding the computed geometries for TS_{Exch} as well as $TS_{G\alpha}$ and $TS_{G\beta}$ with ethanol (Figures 8 and S22–S27), they can be broadly classified as loose (exploded) S_N2 transition states, similar to those previously described by Crich and Bennet for other anomeric substitutions.[10,12] Interestingly, while α-glycosyl triflates evolve through late TSs, characterized by larger distances between the anomeric carbon and the departing group, the corresponding β-anomers progress through early TSs, with shorter distances to the leaving triflate anion. This distinct behavior most probably reflects the operativity of the anomeric effect which renders the α-anomers more stable. As expected, the loose character exhibited by the calculated TSs with ethanol is further exacerbated for the trifluoroethanol reactions. Thus, according to our theoretical calculations, the anomeric substitutions of the β-glycosyl triflates with this acceptor proceed with the concomitant formation of a close-ion pair (β-CIP), now identified as a broad minimum in the reaction coordinate (Figure 8), which is separated from both the starting β-glycosyl triflate and the α-glycosylation product by exceedingly low energy barriers. Of note, the allosyl β-CIP is around 2 kcal/mol more stable than the corresponding glucosyl β-CIP, as previously hypothesized in light of the experimental results. Similar CIP structures could be located by replacing the incoming trifluoroethanol by two solvent molecules (Figure S28), further proving the propensity of β-triflates to form transient formally charged species in the presence of poorly nucleophilic/coordinating additives. Intrinsic reaction coordinate (IRC) calculations proved that very asynchronous but concerted reaction pathways operate for all anomerization and glycosylation reactions except for the α-glycosylations with trifluoroethanol, for which a stepwise inversion mechanism was consistently found (Figure S25). For glucose, this process would be rate-limited by the nucleophilic attack of the alcohol to the contact-ion-pair intermediate ($TS_{G\alpha 2}$) in agreement with a $D_N{}^*A_N{}^{\ddagger}$ mechanism. Indeed, the theoretical KIE calculated at

https://dx.doi.org/10.1021/jacs.0c05525
J. Am. Chem. Soc. 2020, 142, 12501−12514

25 °C for $TS_{G\alpha2}$ amounts to 1.0154, in line with the experimental value. On the contrary, for allose, hydrogen bonding of the alcohol to donor position 3 would lead to a preferential stabilization of $TS_{G\alpha2}$ with respect to $TS_{G\alpha1}$ and a $D_N^{\ddagger}{}^*A_N$ reaction is predicted. However, in this case, the theoretical KIE, derived from $TS_{G\alpha1}$ amounts to 1.0167, showing a larger deviation from the measured value. Most likely, the minute energy differences between $TS_{G\alpha1}$ and $TS_{G\alpha2}$ predicted by the calculations for allose (0.8 kcal/mol at the highest level) renders the distinction between $D_N{}^*A_N^{\ddagger}$ and $D_N^{\ddagger}{}^*A_N$ mechanism extremely difficult to pinpoint.

Overall, the theoretical rendition of the glycosylation reaction presented in this section manages to capture most of the key features experimentally observed for the processes herein described, and supports the atypical mechanistic interpretation inferred from our model systems.

DISCUSSION

The obtained results highlight the mechanistic relevance of β-glycosyl triflates in glycosylation processes, either as reactive intermediates or as reservoirs of even more unstable cationic species, and show that the population and reactivity properties of each anomer together with their mutual exchange dynamics determine to a large extent the stereochemical outcome of the reaction. Regarding β-triflate population, its influence is clearly illustrated by the distinct behavior exhibited by the glucosyl- and mannosyl-triflate mixtures in our competition experiments type ***c-II***: the reaction with ethanol yields β-glycosides with nearly identical rates, while α-product formation is around 10-fold faster for the glucose model, probably reflecting the increased fraction of β-triflate available in this case. Accordingly, this process is further accelerated for the allosyl donor, whose β-triflate equilibrium population is noticeably much higher.

Regarding the intrinsic reactivity properties of the glycosyl triflate intermediates, our competitions type ***c-I*** reveal some general trends which are common for the manno-, gluco-, and allo- donors assayed. Thus, the reaction mechanism leading to the β-products display, in all cases, a significant sensitivity to the nucleophilic character of the acceptor, within the ethanol-trifluoroethanol range, while the opposite is true for the α-stereomers. The simplest interpretation of these observations is that the former derivatives are generated through bimolecular S_N2-like substitutions taking place upon the major, more stable α-glycosyl triflate. On the contrary, α-glycoside formation must involve the participation of more reactive, less discriminating intermediates, such as β-glycosyl-triflates or even β-glycosyl CIPs, which become especially relevant when poor acceptors are employed.

Despite the widespread interest in these latter chemical processes, a detailed picture of the underlying mechanism was still incomplete. With this idea in mind, we set out to dissect two representative examples of these reaction pathways. In the first instance, we focused our attention on the glycosylation of glucose derivative **1a** with trifluoroethanol, which renders a dominant retention α-product from a seemingly exclusive α-glycosyl triflate intermediate. Our second model system was provided by allose donor **8a** and its reaction with the same acceptor. This choice is justified on the basis of chemical considerations, which pointed to an unusually large population of β-triflate intermediate for this particular hexopyranose. Our first efforts were oriented to confirming the presence and, in such case, quantifying the population of these reactive species in the activated reaction mixtures. For the glucose case this goal was achieved by resorting to ^{13}C-labeled samples which allowed us to detect a very minor equilibrium concentration of the β-triflate derivative, thereby defining the equilibrium constant and the free energy gap between both anomers. Regarding the allose donor, NMR experiments not only confirmed our predictions, revealing a remarkably large fraction of the corresponding β-glycosyl triflate in solution, but also allowed the analysis of the anomerization process with unprecedented detail. Hence, equilibrium and kinetic constants were determined under a variety of solvent and temperature conditions. Notably, EXSY NMR experiments performed in the presence of increasing concentration of TBAOTf were consistent with a bimolecular anomerization mechanism.

With this information in hand, the time evolution of glucosyl- and allosyl- triflates upon addition of increasing concentrations of trifluoroethanol was analyzed. The obtained results with both glucose and allose model systems draw a common scenario: the anomeric substitution of the α-glycosyl triflate with anionic triflate to yield the corresponding β-anomer is, in all cases, significantly faster than the reaction with trifluoroethanol to produce the inverted β-glycoside. This observation is in agreement with the reported[21b] relative nucleophilic character of both acceptor species and partially explains the α-stereoselectivity of both glycosylation processes. However, the more unstable β-triflate displays the opposite behavior, showing no preference for any of them, as in the glucose case, or reacting even faster with the alcohol, as in the allose case. Several nonexclusive explanations could account for this latter observation: the nucleophilic attack of the anionic triflate through the α-face of the β-allosyl intermediate is hindered by a polar/steric repulsion with the axially oriented methoxyl substituent at the pyranose position 3, as suggested by the >20-fold drop in the calculated rate constant for this step, $k_{\beta\alpha}$, in comparison with the glucose case. Alternatively, the very same substituent may assist the nucleophilic attack of the neutral alcohol via an intermolecular hydrogen bond interaction, not available for the triflate anion, as supported by our theoretical analysis. According to this view, the hydrogen bonding capacity of the acceptor alcohol (especially that of poor acceptors) would drive the preformation of glycosyl-triflate/acceptor complexes which collapse to the final glycosylation products upon departure of the anomeric leaving group, in line with a S_Ni contribution to the substitution mechanism recently proposed for 3-amino-3-deoxy-allose donors.[25]

Ultimately, the obtained results show that the analyzed glycosylations do not satisfy the Curtin−Hammett boundary requirements for which triflate anomerization should be much faster than the alcohol substitution processes. This conclusion is visually illustrated by the preferential consumption of the β-allosyl triflate over its α-counterpart, which determines that the conversion rate of the α-triflate intermediate into the major retention α-glycoside product is defined by the $\alpha \rightarrow \beta$ triflate anomerization. Such a piece of experimental evidence links the formation of the α-glycoside with the triflate exchange process, implying that the latter can become the rate-limiting step. Additionally, the obtained primary ^{13}C-KIE values point toward very dissociative substitution processes involving oxocarbenium-like reactive species. Altogether, these data support a β-triflate intermediate acting as the exclusive source of β-CIP, whose lifetime must be too short to allow solvent equilibration.[12a]

https://dx.doi.org/10.1021/jacs.0c05525
J. Am. Chem. Soc. 2020, 142, 12501−12514

CONCLUSIONS

Glycosylation reactions involving glycosyl triflate intermediates and weakly nucleophilic alcohols are known to proceed with increased or even complete α-selectivity, presumably reflecting the participation of extremely reactive species, such as the corresponding β-triflates or even glycosyl oxocarbenium ions, otherwise marginally populated in the reaction medium. This evidence has guided the development of new synthetic strategies oriented to directing the stereochemistry of the newly formed glycosidic bonds.[11b] However, a detailed description of the mechanism underlying these processes was still missing. Herein, we have performed a thorough analysis of several paradigmatic and illustrative examples employing a combination of experimental and theoretical chemical approaches that include synthetic chemistry, NMR, kinetic analysis, and computational studies. Despite the highly dissociative character assigned to these processes, which probably involve a β-CIP as the reacting donor species, the obtained results provide support for the key role of the β-triflates as a cornerstone in α-glycosylations. Therefore, the S_N2-like anomerization of the preponderant α-triflate represents an essential step which necessarily precedes glycosidic bond formation. Strikingly, under certain experimental circumstances, weak acceptor alcohols can indeed outcompete the triflate anion in the β-triflate substitution, thus turning the glycosyl triflate exchange into the rate-determining step. In our opinion, this behavior reflects the distinct properties of neutral and charged nucleophiles under the low polarity/low temperature conditions commonly employed in glycosylations. Against common belief, and according to our data, only extraordinarily weak alcohols (i.e., HFIP) react within Curtin–Hammett boundary conditions.

ASSOCIATED CONTENT

Supporting Information

The Supporting Information is available free of charge at https://pubs.acs.org/doi/10.1021/jacs.0c05525.

Detailed description of the experimental methods and synthetic protocols together with the characterization of products and intermediates; Figures S1–S29 with details of the NMR, reactivity experiments, and QM calculations (PDF)

AUTHOR INFORMATION

Corresponding Author

Juan Luis Asensio – *Instituto de Química Orgánica (IQOG-CSIC), 28006 Madrid, Spain;* orcid.org/0000-0001-7536-5221; Email: juanluis.asensio@csic.es

Authors

Andrés G. Santana – *Instituto de Química Orgánica (IQOG-CSIC), 28006 Madrid, Spain;* orcid.org/0000-0003-3568-7714

Laura Montalvillo-Jiménez – *Instituto de Química Orgánica (IQOG-CSIC), 28006 Madrid, Spain*

Laura Díaz-Casado – *Instituto de Química Orgánica (IQOG-CSIC), 28006 Madrid, Spain*

Francisco Corzana – *Departamento Química and Centro de Investigación en Síntesis Química, Universidad de La Rioja, 26006 Rioja, Spain;* orcid.org/0000-0001-5597-8127

Pedro Merino – *Instituto de Biocomputación y Física de Sistemas Complejos (BIFI), Universidad de Zaragoza, 50018 Zaragoza, Spain;* orcid.org/0000-0002-2202-3460

Francisco J. Cañada – *Centro de Investigaciones Biológicas (CIB-CSIC), 28040 Madrid, Spain*

Gonzalo Jiménez-Osés – *Center for Cooperative Research in Biosciences (CIC-bioGUNE), 48160 Derio, Spain;* orcid.org/0000-0003-0105-4337

Jesús Jiménez-Barbero – *Center for Cooperative Research in Biosciences (CIC-bioGUNE), 48160 Derio, Spain; Ikerbasque Basque Foundation for Science, 48013 Bilbao, Basque;* orcid.org/0000-0001-5421-8513

Ana M. Gómez – *Instituto de Química Orgánica (IQOG-CSIC), 28006 Madrid, Spain;* orcid.org/0000-0002-8703-3360

Complete contact information is available at: https://pubs.acs.org/10.1021/jacs.0c05525

Author Contributions

[▽]These authors contributed equally to this work.

Funding

This investigation was supported by research grants from the Spanish Ministry of Science and Innovation (CTQ2016–79255-P, PID2019–107476GB-I00, BFU2017–89707-P, RTI2018–094862-B-100, RTI2018–099592–B-C21, PID2019–104090RB-100, RTI2018–094751–B-C22, and RTI2018–099592–B-C22), the Mizutani Foundation for Glycoscience (200077 and 170045), the Aragon Government (Groups 17R-34) and the computational resources from BIFI-ZCAM (Universidad de Zaragoza, Spain).

Notes

The authors declare no competing financial interest.

ACKNOWLEDGMENTS

A.G.S. would like to thank the EU commission for a MSCA-IF postdoctoral fellowship. L.M.-J and L.D.-C thank the Ministerio de Economía, Industria y Competitividad and the Ministerio de Ciencia, Innovación y Universidades the for their FPI fellowships (BES-2014-070232 and BES-2017-080618). NMR experiments were performed in the "Manuel Rico" NMR laboratory (LMR) of the Spanish National Research Council (CSIC), a node of the Spanish Large Scale National facility (ICTS-R-LRB).

REFERENCES

(1) Kulkarni, S. S.; Wang, C.-C.; Sabbavarapu, N. M.; Podilapu, A. R.; Liao, P.-H.; Hung, S.-C. One-Pot" Protection, Glycosylation, and Protection–Glycosylation Strategies of Carbohydrates. *Chem. Rev.* **2018**, *118* (17), 8025–8104.

(2) Nielsen, M. M.; Pedersen, M. C. Catalytic Glycosylations in Oligosaccharide Synthesis. *Chem. Rev.* **2018**, *118* (17), 8285–8358.

(3) Leng, W. L.; Yao, H.; He, J. X.; Liu, X. W. Venturing beyond Donor-Controlled Glycosylation: New Perspectives toward Anomeric Selectivity. *Acc. Chem. Res.* **2018**, *51* (3), 628–639.

(4) (a) Yu, B. Gold(I)-Catalyzed Glycosylation with Glycosyl o-Alkynylbenzoates as Donors. *Acc. Chem. Res.* **2018**, *51* (2), 507–516. (b) Yu, B.; Sun, J.; Yang, X. Assembly of Naturally Occurring Glycosides, Evolved Tactics, and Glycosylation Methods. *Acc. Chem. Res.* **2012**, *45* (8), 1227–1236.

(5) Chen, J.; Hansen, T.; Zhang, Q. J.; Liu, D. Y.; Sun, Y.; Yan, H.; Codée, J. D. C.; Schmidt, R. R.; Sun, J. S. 1-Picolinyl-5-azido Thiosialosides: Versatile Donors for the Stereoselective Construction of Sialyl Linkages. *Angew. Chem., Int. Ed.* **2019**, *58* (47), 17000–17008. (b) Wang, L.; Overkleeft, H. S.; van der Marel, G. A.; Codée, J. D. C. Reagent Controlled Stereoselective Synthesis of α-Glucans. *J. Am. Chem. Soc.* **2018**, *140* (14), 4632–4638.

(6) Guberman, M.; Seeberger, P. H. Automated Glycan Assembly: A Perspective. *J. Am. Chem. Soc.* **2019**, *141* (14), 5581–5592.

(7) Chang, C. W.; Wu, C. H.; Lin, M. H.; Liao, P. H.; Chang, C. H.; Chuang, H. H.; Lin, S. C.; Lam, S.; Verma, V. P.; Hsu, C. P.; Wang, C. C. Establishment of Guidelines for the Control of Glycosylation Reactions and Intermediates by Quantitative Assessment of Reactivity. *Angew. Chem., Int. Ed.* **2019**, *58*, 16775−16779.
(8) Bennett, C. S.; Galan, M. C. Methods for 2-Deoxyglycoside Synthesis. *Chem. Rev.* **2018**, *118*, 7931.
(9) Zhang, Y.; Gomez-Redondo, M.; Jimenez-Oses, G.; Arda, A.; Overkleeft, H. S.; Marel, G. A.; Jimenez-Barbero, J.; Codee, J. D. C. Synthesis and Structural Analysis of Aspergillus fumigatus Galactosaminogalactans featuring α-galactose, α-galactosamine and α-N-acetyl galactosamine linkages. *Angew. Chem., Int. Ed.* **2020**, *59*, 1−6.
(10) (a) Adero, P. O.; Amarasekara, H.; Wen, P.; Bohé, L.; Crich, D. The Experimental Evidence in Support of Glycosylation Mechanisms at the S_N1-S_N2 Interface. *Chem. Rev.* **2018**, *118*, 8242−8284. (b) Adero, P. O.; Furukawa, T.; Huang, M.; Mukherjee, D.; Retailleau, P.; Bohé, L.; Crich, D. Cation Clock Reactions for the Determination of Relative Reaction Kinetics in Glycosylation Reactions: Applications to Gluco- and Mannopyranosyl Sulfoxide and Trichloroacetimidate Type Donors. *J. Am. Chem. Soc.* **2015**, *137*, 10336−10345. (c) Huang, M.; Retailleau, P.; Bohé, L.; Crich, D. Cation Clock Permits Distinction Between the Mechanisms of α- and β-O- and β-C-Glycosylation in the Mannopyranose Series: Evidence for the Existence of a Mannopyranosyl Oxocarbenium Ion. *J. Am. Chem. Soc.* **2012**, *134*, 14746−14749. (d) Huang, M.; Garrett, G. E.; Birlirakis, N.; Bohé, L.; Pratt, D. A.; Crich, D. Dissecting the mechanisms of a class of chemical glycosylation using primary ^{13}C kinetic isotope effects. *Nat. Chem.* **2012**, *4*, 663−667. (e) Crich, D. Mechanism of a chemical glycosylation reaction. *Acc. Chem. Res.* **2010**, *43*, 1144−1153. (f) Crich, D.; Chandrasekera, N. S. Mechanism of 4,6-*O*-Benzylidene-Directed β-Mannosylation as Determined by α-Deuterium Kinetic Isotope Effects. *Angew. Chem., Int. Ed.* **2004**, *43*, 5386−5389.
(11) (a) van der Vorm, S.; Hansen, T.; Overkleeft, H. S.; van der Marel, G. A.; Codẽe, J. D. C. The influence of acceptor nucleophilicity on the glycosylation reaction mechanism. *Chem. Sci.* **2017**, *8*, 1867−1875. (b) van der Vorm, S.; van Hengst, J. M. A.; Bakker, M.; Overkleeft, H. S.; van der Marel, G. A.; Codée, J. D. C. Mapping the Relationship between Glycosyl Acceptor Reactivity and Glycosylation Stereoselectivity. *Angew. Chem., Int. Ed.* **2018**, *57*, 8240−8244. (c) van Rijssel, E. R.; van Delft, P.; Lodder, G.; Overkleeft, H. S.; van der Marel, G. A.; Filippov, D. V.; Codẽe, J. D. C. Furanosyl Oxocarbenium Ion Stability and Stereoselectivity. *Angew. Chem., Int. Ed.* **2014**, *53*, 10381−10385.
(12) (a) Colombo, C.; Bennet, A. J. The physical organic chemistry of glycopyranosyl transfer reactions in solution and enzyme-catalyzed. *Curr. Opin. Chem. Biol.* **2019**, *53*, 145−157. (b) Chan, J.; Tang, A.; Bennet, A. J. A Stepwise Solvent-Promoted S_Ni Reaction of α-D-Glucopyranosyl Fluoride: Mechanistic Implications for Retaining Glycosyltransferases. *J. Am. Chem. Soc.* **2012**, *134*, 1212−1220. (c) Bennet, A. J.; Sinnott, M. L. Complete kinetic isotope effect description of transition states for acid-catalyzed hydrolyses of methyl α- and βglucopyranosides. *J. Am. Chem. Soc.* **1986**, *108*, 7287−7294. (d) Namchuk, M. N.; McCarter, J. D.; Becalski, A.; Andrews, T.; Withers, S. G. The Role of Sugar Substituents in Glycoside Hydrolysis. *J. Am. Chem. Soc.* **2000**, *122*, 1270−1277. (e) Beaver, M. G.; Buscagan, T. M.; Lavinda, O.; Woerpel, K. A. Stereoelectronic Model to Explain Highly Stereoselective Reactions of Seven-Membered-Ring Oxocarbenium-Ion Intermediates. *Angew. Chem., Int. Ed.* **2016**, *55*, 1816−1819. (f) Smith, D. M.; Woerpel, K. A. Electrostatic interactions in cations and their importance in biology and chemistry. *Org. Biomol. Chem.* **2006**, *4*, 1195−1201. (g) Ayala, L.; Lucero, C. G.; Romero, J. A. C.; Tabacco, S. A.; Woerpel, K. A. Stereochemistry of Nucleophilic Substitution Reactions Depending upon Substituent: Evidence for Electrostatic Stabilization of Pseudoaxial Conformers of Oxocarbenium Ions by Heteroatom Substituents. *J. Am. Chem. Soc.* **2003**, *125*, 15521−15528.
(13) (a) Marianski, M.; Mucha, E.; Greis, K.; Moon, S.; Pardo, A.; Kirschbaum, C.; Thomas, D. A.; Meijer, G.; Helden, G.; Gilmore, K.; Seeberger, P. H.; Pagel, K. Remote Participation during Glycosylation Reactions of Galactose Building Blocks: Direct Evidence from Cryogenic Vibrational Spectroscopy. *Angew. Chem., Int. Ed.* **2020**, *59*, 6166−6171. (b) Chatterjee, S.; Moon, S.; Hentschel, F.; Gilmore, K.; Seeberger, P. H. An Empirical Understanding of the Glycosylation Reaction. *J. Am. Chem. Soc.* **2018**, *140*, 11942−11953.
(14) (a) Frihed, T. G.; Bols, M.; Pedersen, C. M. Mechanisms of Glycosylation Reactions Studied by Low Temperature Nuclear Magnetic Resonance. *Chem. Rev.* **2015**, *115*, 4963−5013. (b) Heuckendorff, M.; Bols, P. S.; Barry, C. B.; Frihed, T. G.; Pedersen, C. M.; Bols, M. ,-Mannosylation with 4,6-benzylidene protected mannosyl donors without preactivation. *Chem. Commun.* **2015**, *51*, 13283−13285.
(15) (a) Lebedel, L.; Ardá, A.; Martin, A.; Désiré, J.; Mingot, A.; Aufiero, M.; Aiguabella Font, N.; Gilmour, R.; Jiménez-Barbero, J.; Blériot, Y.; Thibaudeau, S. Structural and Computational Analysis of 2-Halogeno-Glycosyl Cations in the Presence of a Superacid: An Expansive Platform. *Angew. Chem., Int. Ed.* **2019**, *58* (39), 13758−13762. (b) Martin, A.; Ardá, A.; Désiré, J.; Martin-Mingot, A.; Probst, N.; Sinaÿ, P.; Jiménez-Barbero, J.; Thibaudeau, S.; Blériot, Y. Catching elusive glycosyl cations in a condensed phase with HF/SbF5 superacid. *Nat. Chem.* **2016**, *8* (2), 186−191.
(16) (a) Crich, D.; Sun, S. Direct chemical synthesis of β-mannopyranosides and other glycosides via glycosyl triflates. *Tetrahedron* **1998**, *54* (29), 8321−8348. (b) Crich, D.; Sun, S.; Yu, B.; Dai, L. X. Glycosyl triflates are intermediates that lead to an efficient protocol for β-mannopyranoside formation from thioglycosides. *Chemtracts* **1999**, *12* (9), 629−634. (c) Crich, D.; Smith, M. S-(4-methoxyphenyl)benzenethiosulfinate (MPBT)/trifluoromethanesulfonic anhydride: A convenient system for the generation of glycosyl triflates from thioglycosides. *Org. Lett.* **2000**, *2* (25), 4067−4069. (d) Nokami, T.; Shibuya, A.; Tsuyama, H.; Suga, S.; Bowers, A. A.; Crich, D.; Yoshida, J. I. Electrochemical generation of glycosyl triflate pools. *J. Am. Chem. Soc.* **2007**, *129* (35), 10922−10928. (e) Crich, D.; Sun, S. Are Glycosyl Triflates Intermediates in the Sulfoxide Glycosylation Method? A Chemical and ^{1}H, ^{13}C, and ^{19}F NMR Spectroscopic Investigation. *J. Am. Chem. Soc.* **1997**, *119* (46), 11217−11223.
(17) The Anomeric Effect and Associated Stereoelectronic Effects. *ACS Symposium Series 539*; Thatcher, G. R. J., Ed.; American Chemical Society: Washington, DC, 1993.
(18) (a) Walvoort, M. T. C.; Lodder, G.; Mazurek, J.; Overkleeft, H. S.; Codée, J. D. C.; van der Marel, G. A. Equatorial Anomeric Triflates from Mannuronic Acid Esters. *J. Am. Chem. Soc.* **2009**, *131*, 12080−12081. (b) Rönnols, J.; Walvoort, M. T. C.; van der Marel, G. A.; Codée, J. D. C.; Widmalm, G. Chair interconversion and reactivity of mannuronic acid esters. *Org. Biomol. Chem.* **2013**, *11*, 8127−8134.
(19) (a) Sinnott, M. L.; Jencks, W. P. Solvolysis of D-glucopyranosyl derivatives in mixtures of ethanol and 2,2,2-trifluoroethanol. *J. Am. Chem. Soc.* **1980**, *102* (6), 2026−2032. (b) Beaver, M. G.; Woerpel, K. A. Erosion of Stereochemical Control with Increasing Nucleophilicity: O-Glycosylation at the Diffusion Limit. *J. Org. Chem.* **2010**, *75*, 1107−1118.
(20) Kuzmic, P. Program DYNAFIT for the Analysis of Enzyme Kinetic Data: Application to HIV Proteinase. *Anal. Biochem.* **1996**, *237*, 260−273.
(21) (a) Dhakal, B.; Bohé, L.; Crich, D. Trifluoromethanesulfonate Anion as Nucleophile in Organic Chemistry. *J. Org. Chem.* **2017**, *82*, 9263−9269. (b) Kiyooka, S.-I.; Kaneno, D.; Fujiyama, R. Intrinsic reactivity index as a single scale directed toward both electrophilicity and nucleophilicity using frontier molecular orbitals. *Tetrahedron* **2013**, *69*, 4247−4258.
(22) (a) Haindl, M. H.; Hioe, J.; Gschwind, R. M. The Proline Enamine Formation Pathway Revisited in Dimethyl Sulfoxide: Rate Constants Determined via NMR. *J. Am. Chem. Soc.* **2015**, *137*, 12835−12842. (b) D'Angelo, K. A.; Taylor, M. S. Borinic Acid Catalyzed Stereo- and Regioselective Couplings of Glycosyl Methanesulfonates. *J. Am. Chem. Soc.* **2016**, *138*, 11058−11066.
(23) (a) Singleton, D. A.; Szymanski, M. J. Simultaneous determination of intermolecular and intramolecular ^{13}C and ^{2}H kinetic

https://dx.doi.org/10.1021/jacs.0c05525
J. Am. Chem. Soc. 2020, 142, 12501−12514

isotope effects at natural abundance. *J. Am. Chem. Soc.* **1999**, *121*, 9455−9456. (b) Singleton, D. A.; Szymanski, M. J. High-Precision Simultaneous Determination of Multiple Small Kinetic Isotope Effects at Natural Abundance. *J. Am. Chem. Soc.* **1999**, *121*, 9455−9456.
(24) Jensen, H. H.; Bols, M. Stereoelectronic Substituent Effects. *Acc. Chem. Res.* **2006**, *39*, 259−265.
(25) Zeng, J.; Wang, R.; Zhang, S.; Fang, J.; Liu, S.; Sun, G.; Xu, B.; Xiao, Y.; Fu, D.; Zhang, W.; Hu, Y.; Wan, Q. Hydrogen-Bonding-Assisted Exogenous Nucleophilic Reagent Effect for β-Selective Glycosylation of Rare 3-Amino Sugars. *J. Am. Chem. Soc.* **2019**, *141* (21), 8509−8515.

https://dx.doi.org/10.1021/jacs.0c05525
J. Am. Chem. Soc. 2020, 142, 12501−12514